

Pathway to an excitonic coherence

V. Laurindo Jr., E. D. Guarin Castro, G. M. Jacobsen, E. R. C. de Oliveira, J.

F. M. Domenegueti, G. E. Marques, M. D. Teodoro,* and V. Lopez-Richard†

Departamento de Física, Universidade Federal de São Carlos, 13565-905, São Carlos, SP, Brazil

B. Alén

*Instituto de Micro y Nanotecnología, IMN-CNM,
CSIC (CEI UAM + CSIC), Tres Cantos, E-28760, Madrid, Spain*

Yu. I. Mazur and G. J. Salamo

Institute for Nanoscience and Engineering, University of Arkansas, Fayetteville, 72701, Arkansas, USA

E. Marega Jr.

Instituto de Física de São Carlos, Universidade de São Paulo, 13566-590, São Carlos, SP, Brazil

(Dated: July 6, 2021)

This paper discusses the combined effects of optical excitation power, interface roughness, lattice temperature, and applied magnetic fields on the spin-coherence of excitonic states in GaAs/AlGaAs multiple quantum wells. For low optical powers, at lattice temperatures between 4 K and 50 K, the scattering with acoustic phonons and short-range interactions appear as the main decoherence mechanisms. Statistical fluctuations of the band-gap however become also relevant in this regime and we were able to deconvolute them from the decoherence contributions. The circularly polarized magneto-photoluminescence unveils a non-monotonic tuning of the coherence for one of the spin components at low magnetic fields. This effect has been ascribed to the competition between short-range interactions and spin-flip scattering, modulated by the momentum relaxation time.

I. INTRODUCTION

Electronic spin in semiconductors has become a potential building block for applications in spintronics and quantum information technologies.[1, 2] This has been studied in a variety of semiconductor platforms ranging from the traditional III-V and II-VI groups to monolayers of transition-metal dichalcogenides [3–6] and significant efforts have been devoted to controlling and increasing the spin coherence time. [7–9]

Under a non-resonant optical excitation regime, photo-generated spin carriers subsequently lose energy by scattering processes followed by exciton radiative recombination. This photoluminescence (PL) is mediated by decoherence mechanisms that broaden the exciton linewidth, providing information on the time scale in which the exciton can be coherently manipulated. [10] Under an external applied magnetic field, the additional confinement in xy -plane can tune the scattering processes, also increasing the exciton spin relaxation time [11] that could lead to spontaneous coherence. [12–15] Therefore, there is an active search for understanding how and under which conditions different decoherence mechanisms of excitons are triggered. To answer these questions we investigated the relaxation process of excitons and the effect of external magnetic fields on the tuning of the spin-coherence in quantum wells (QWs). By reducing the lattice tempera-

ture and for low excitation powers, the presence of band-gap fluctuations stabilizes the effective carriers temperature at values higher than the lattice temperature. By applying a magnetic field in this regime, the exciton spin coherence can be tuned. In this case, the combination of short-range interactions and spin-flip scattering is the leading mechanism as supported by our simulations.

II. SAMPLE AND EXPERIMENTAL SETUP

A multiple QW heterostructure was grown via molecular-beam epitaxy on an undoped GaAs(100) substrate, consisting of twenty QWs with individual width of 55 Å and Al_{0.36}Ga_{0.64}As barriers with individual thickness of ~ 300 Å - thick enough to avoid carrier tunneling between consecutive wells. Continuous-wave PL measurements were performed by means of a confocal microscope with samples placed inside a magneto-optical cryostat (Attocube/Attodry 1000), with temperatures ranging from 3.6 K to 80 K, and magnetic fields up to 6 T. Time-resolved PL as a function of the magnetic field was also measured at the lowest temperature. A linear polarized diode laser (PicoQuant LDH Series) were used as an excitation source ($\lambda = 730$ nm) at a repetition rate of 80 MHz focused on a spot diameter of ~ 1 μ m. A set of polarizers was used in order to identify the correspondent sigma plus (σ^+) and minus (σ^-) optical component emissions from the sample, which were dispersed by a 75 cm spectrometer (Andor / Shamrock), detected in continuous wave mode by a Silicon CCD (Andor / Idus) and in time-resolved mode by a hybrid PMT (PicoQuant) and a

* mdaldin@gmail.com

† vlopez@df.ufscar.br

time-correlated single-photon counting device (PicoHarp 300).

III. RESULTS AND DISCUSSION

The PL spectra at a lattice temperature of $T_L = 3.6$ K are presented in Fig. 1a for various laser power densities. Here, the main electron-heavy hole emission peak at 1.615 eV, labeled as e-hh, corresponds to the $1s$ ground state recombination. [16] At high laser power densities an emission at 1.621 eV, labeled as e-hh1, is ascribed to the $2s$ exciton state. [16, 17] The e-hh spectral tail in Fig. 1a follows a Boltzmann distribution, $f \propto \exp(-\hbar\omega/k_B T_{\text{eff}})$ where $\hbar\omega$ is the emitted photon energy while T_{eff} is the hot-exciton effective temperature. The value of $1/T_{\text{eff}}$ extracted from the e-hh emission tail is presented in Fig. 1b as a function of the photon flux density defined as $F = P/(\hbar\omega_l)$, with P being the laser power density and $\hbar\omega_l$ the laser energy. [18] In Fig. 1b, the flux density has been normalized to the maximum value of the experimental range, $\tilde{F} = F/F_{\text{max}}$ for two different lattice temperatures.

When the longitudinal optical (LO-)phonon scattering is the most efficient energy relaxation process, the relation $F \propto \exp[-\hbar\omega_{\text{LO}}/(k_B T_{\text{eff}})]$ is expected, with $\hbar\omega_{\text{LO}} = 36.5$ meV being the LO-phonon energy in GaAs. [18] This is depicted in Fig. 1b by solid lines, in good agreement with the experimental data at high incident photon fluxes ($\tilde{F} > 10^{-3}$). At low optical power densities the effective temperature deviates from this trend, stabilizing at a constant value of 17 K for $T_L = 3.6$ K, and 19 K for $T_L = 10$ K. This points to a constriction of the LO-phonon scattering, enhancing the relative contribution of the carrier-carrier interaction which stabilizes the effective temperature. [19] As demonstrated below, this constriction is triggered in the regime where the energy band-gap fluctuations, caused by roughness at the GaAs/AlGaAs interfaces [20] play a dominant role. [21]

The PL spectra obtained with a laser power density of 60 W/cm^2 are shown in Fig. 1c varying T_L . In this case the e-hh1 emission is well resolved and T_{eff} is displayed in Fig. 1d for both e-hh and the e-hh1 tails as a function of T_L . The condition of perfect thermalization with the lattice, $T_{\text{eff}} = T_L$, is also represented. The excited states show higher temperatures than the ground state and by increasing T_L a more efficient thermalization with the lattice is observed. We should note that for temperatures above 25 K, the e-hh tail exhibits a shoulder around 1.620 eV that hampers the extraction of reliable values of T_{eff} . The stabilization of the effective temperature at lower lattice temperatures points to the constriction of phonon-mediated relaxation that hampers the thermalization with the lattice.

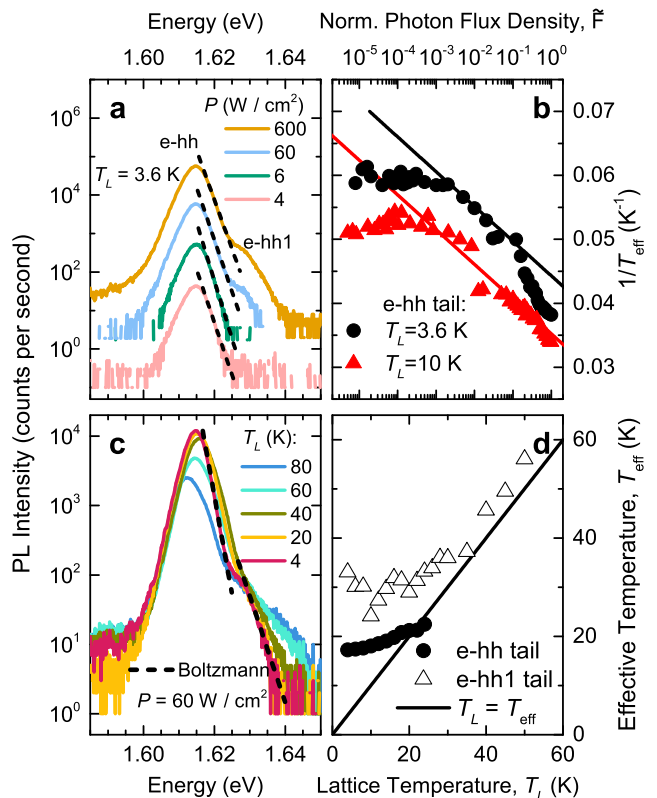


FIG. 1. (a) PL spectra emission for different laser ($\hbar\omega_l = 1.69$ eV) power densities at a lattice temperature of 3.6 K. (b) Inverse of the effective temperature obtained from the e-hh spectral tail versus the normalized photon flux density, \tilde{F} , at a lattice temperature of 3.6 K and 10 K. Solid lines simulate the effective temperature variation produced by LO-phonon scattering, $F \propto \exp[-\hbar\omega_{\text{LO}}/(k_B T_{\text{eff}})]$. (c) PL spectra for different lattice temperatures at a constant laser power density of 60 W/cm^2 . The high-energy side of the e-hh and e-hh1 emissions were fitted using Boltzmann functions (dashed lines). (d) Effective temperature obtained from the e-hh and e-hh1 spectral tails as a function of the lattice temperature. Solid line represents the case of carriers thermalization with the lattice ($T_{\text{eff}} = T_L$).

A. Exciton relaxation dynamics.

For assessing the relative role of different decoherence mechanisms, the full width at half maximum (FWHM) of the emission lines can be examined. Although the coherence loss by time-irreversible processes can be mapped by analyzing how the FWHM changes with temperature and external fields, this parameter is also affected by statistical fluctuations of the spatial variation of the light sources (excitons in this case). So the role played by the statistics of the interface roughness must be determined.

In order to assess this effect, the lattice temperature dependence of the e-hh peak position, E_p , has been displayed in Fig. 2a for two laser power densities along with

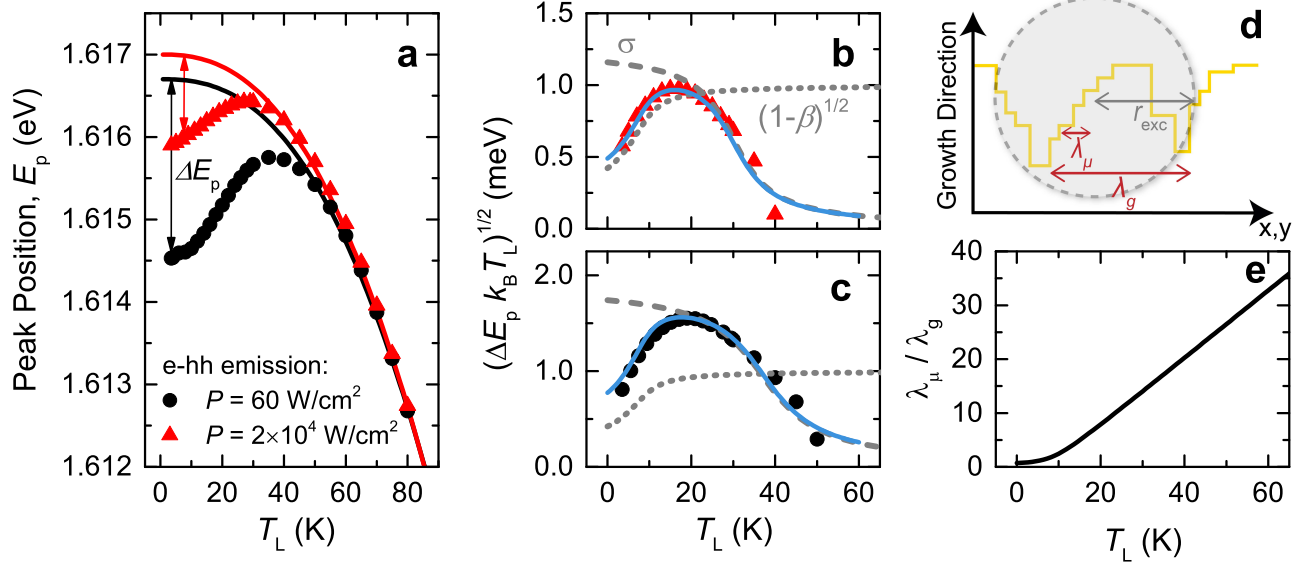


FIG. 2. (a) PL peak energy, E_p , as a function of temperature for laser power densities of $2 \times 10^4 \text{ W/cm}^2$ and 60 W/cm^2 . Solid curves represent the simulations based on Eq. 1. Temperature dependence of $\sqrt{\Delta E_p k_B T_L} \simeq \sigma \sqrt{1 - \beta}$ for (b) $P = 2 \times 10^4 \text{ W/cm}^2$ and (c) $P = 60 \text{ W/cm}^2$. Simulations (solid blue lines) were obtained by using step-like functions for σ (dashed line) and $(1 - \beta)^{1/2}$ (dotted line). (d) Schematic representation of the characteristic lengths of the band gap fluctuations, λ_μ and λ_g , as compared with the excitonic radius, r_{exc} . (e) Temperature dependence of the λ_μ/λ_g ratio calculated from the β obtained in (b) and (c).

simulations using the expression [22]

$$E_p(T_L) = E_g - \frac{\alpha\Theta}{2} \left[\sqrt[p]{1 + \left(\frac{2T_L}{\Theta}\right)^p} - 1 \right] + E_{\text{exc}}, \quad (1)$$

where $E_g = 1.519 \text{ eV}$ is the GaAs energy band-gap at $T_L = 0 \text{ K}$, and $E_{\text{exc}} = 98 \text{ meV}$ is the extra energy given by the QW confinement, $\alpha = 5.405 \times 10^{-4} \text{ eV/K}$, [23] $\Theta = 418 \text{ K}$ is the effective phonon temperature, while $p = 2.5$ for 60 W/cm^2 and $p = 2.45$ for $2 \times 10^4 \text{ W/cm}^2$. Here, p is a parameter related to the shape of the electron-phonon spectral function. [22, 24] The deviation, ΔE_p , of the theoretical expectations and the experiment, is produced by local band-gap fluctuations provoked by interface roughness. [24] At low temperatures, excitons can be trapped into these fluctuations and, by increasing T_L , they progressively diffuse and recombine radiatively from higher energy states. By increasing the laser power density [24] the band-gap fluctuations are effectively screened reducing ΔE_p , as confirmed in Figs. 2a, b and c. These effects can be analyzed by using the model reported in Ref. 25, which describes the emission intensity as a function of the photon energy E , as

$$\phi(E) = \text{erfc} \left(\frac{E_g - E + \beta\sigma^2/k_B T_L}{\sqrt{2}\sigma} \right) E^2 \exp \left(-\frac{E - \mu_0 - \beta E_g}{k_B T_L} + \frac{\beta^2 \sigma^2}{2(k_B T_L)^2} \right), \quad (2)$$

where σ is the standard deviation of the local band-gap fluctuations, [24, 26] and $\beta = [1 + (\lambda_\mu/\lambda_g)^2]^{-1/2} \in (0, 1]$

depends on the ratio of the characteristic length of the carriers transport, λ_μ , with respect to the correlation length scale of the fluctuations, λ_g , and ponders the trapping efficiency: $\beta \rightarrow 0$, small-scale fluctuations (inefficient trapping) and $\beta = 1$, large-scale fluctuations (efficient trapping). This has been schematically represented in Figs. 2d.

For relatively large arguments of the complementary error function, $\text{erfc}(z) \approx \exp(-z^2)/\sqrt{\pi}z$, [27] and the intensity becomes proportional to

$$\phi(E) \propto \exp \left(-\frac{E_g - \frac{\sigma^2}{k_B T_L}(1 - \beta) - E}{2\sigma^2} \right). \quad (3)$$

Thus, for relatively low temperatures, its contribution to the FWHM is determined by the standard deviation of the gap fluctuation as $W_\sigma = 2\sqrt{2 \ln 2} \cdot \sigma$ while ΔE_p can be approximated as

$$\Delta E_p(T_L) \simeq \frac{\sigma^2}{k_B T_L} (1 - \beta). \quad (4)$$

After extracting the difference between Eq. 1 and the experimental data, the value of $\sqrt{\Delta E_p(T_L) k_B T_L} = \sigma \sqrt{1 - \beta}$ has been displayed in Figs. 2b and c for $P = 2 \times 10^4 \text{ W/cm}^2$ and $P = 60 \text{ W/cm}^2$, respectively, showing a nonmonotonic behavior between 4 and 50 K. The corresponding experimental values of FWHM have been obtained by a Gaussian fitting of the e-hh emission as a function of T_L for the case of $P = 60 \text{ W/cm}^2$ and displayed in Fig. 3a. In this case a bump appears in the

temperature range where the gap fluctuation effects are more evident. Since both, power and temperature, affect the way the fluctuations are screened, they can also tune the effective values of both, σ and β . Increasing power and/or temperature provokes an apparent homogenization of the fluctuations (through screening), reducing σ while favoring exciton diffusion that translates into a β decrease. By assuming σ and β as soft step-like functions so that $\sigma, \beta \rightarrow 0$ for growing T_L with maximal σ and $\beta \rightarrow 1$ for $T_L \rightarrow 0$, then σ decreases by increasing T_L while $\sqrt{1-\beta}$ grows, as illustrated in Figs. 2b and c. The product $\sigma\sqrt{1-\beta}$ is also represented reproducing the nonmonotonic behavior of $\sqrt{\Delta E_p(T_L)k_B T_L}$ up to temperatures between 40 and 50 K. The function used to emulate β dependence on temperature has been the same in panels b and c of Fig. 2 and this allows extracting the expected ratio λ_μ/λ_g that was depicted in panel e. This suggests an increased detrapping as the temperature grows.

In the case of the FWHM, displayed in Fig. 3a, the analysis of the temperature modulation must also include the tuning of the homogeneous lifetime broadening. Thus, assuming the homogeneous broadening as a Lorentzian width, W_h , and the inhomogeneous fluctuations characterized by a Gaussian width, $W_\sigma = 2\sqrt{2\ln 2} \cdot \sigma$, their relative contribution to the FWHM can be approximated as a Voigt convolution, [28, 29]

$$\text{FWHM} = \frac{W_h}{2} + \sqrt{\frac{W_h^2}{4} + W_\sigma^2}. \quad (5)$$

The homogeneous broadening can be simulated by considering different independent and additive mechanisms [21] that, for low temperatures, can be reduced to two,

$$W_h = \Gamma_0 + \Gamma_{LA}, \quad (6)$$

where Γ_0 represents the intrinsic 2D-excitonic linewidth, associated to exciton-exciton and defects scattering; [19, 21] and $\Gamma_{LA} = 2\gamma_a T_L$ arises from LA-phonon scattering. For the function σ used previously, the best simulation of FWHM was obtained using $\Gamma_0 = 4.7$ meV and $\gamma_a = 11$ $\mu\text{eV}/\text{K}$, as displayed in Fig. 3a. The parameter γ_a which characterizes the exciton-phonon coupling strength is almost 10 times larger than reported values for other GaAs quantum well structures, [21, 30] but of the same order of magnitude of other semiconductor layered systems. [10, 19, 31] Note that the simulation and the experimental values disagree for lower temperatures. As displayed in Fig. 3b, by comparing the results using Eq. 2 and the approximation of Eq. 3 this latter does not account for the whole characterization of the spectral width modulation with temperature. A small but discernible modulation, for constant σ , already occurs at low T_L . As predicted in Ref. 30, the LO-phonon scattering and ionized impurities interaction do not significantly contribute to the broadening of the linewidth within the temperature range analyzed, while LA-phonon interaction is the dominant scattering mechanism above 40 K.

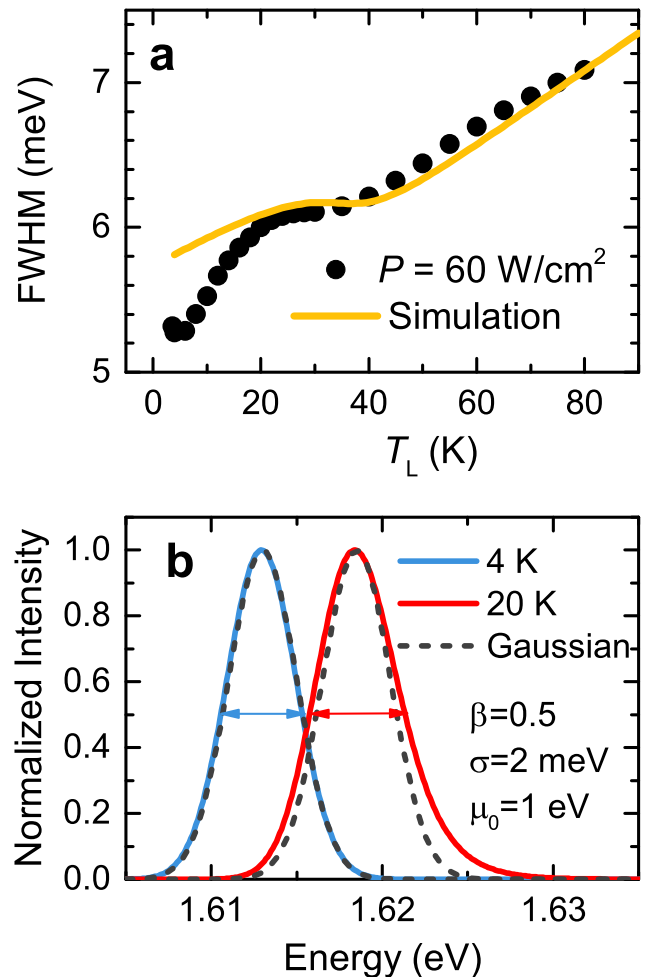


FIG. 3. (a) FWHM as a function of the lattice temperature for the e-hh emission and $P = 60$ W/cm^2 (dots). The simulated FWHM considering homogeneous and inhomogeneous contributions is also displayed (yellow line). (b) Simulated PL spectra with the same σ and β for $T_L = 4$ K (blue line) and $T_L = 10$ K (red line), obtained using Eq. 2 and Gaussian functions (dashed lines) according to Eq. 3.

For $T_L < 40$ K, band-gap fluctuations broadening dominates and responds for the observed bump that can be ascribed to their effective homogenization as σ decreases with T_L .

B. Quantum coherence mechanisms in magnetic fields

At cryogenic temperatures, phonon-assisted decoherence mechanisms are constricted. This opens the opportunity for studying the scattering processes in the presence of magnetic fields that tune the exciton size [32–34] and the exciton spin relaxation [11, 35] allowing for additional modulation of the exciton coherence. Figures 4a and b display, respectively, the integrated intensity and FWHM of the e-hh σ^+ and σ^- optical compo-

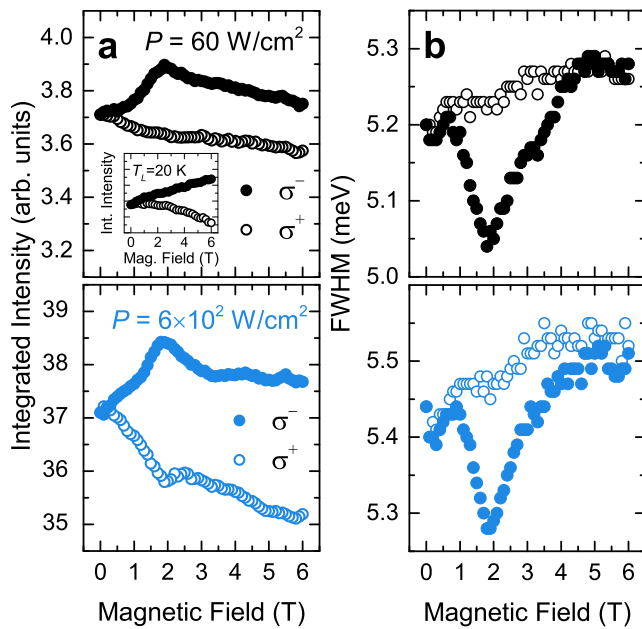


FIG. 4. Magnetic field dependence of: (a) integrated intensity, and (b) FWHM of the e-hh emission at $T_L = 3.6$ K, obtained with $P = 60$ W/cm 2 (top panels) and $P = 6 \times 10^2$ W/cm 2 (bottom panels). Solid and open circles represent the responses measured from σ^- and σ^+ optical component emissions, respectively. The inset in (a) shows the integrated intensity observed at $T_L = 20$ K.

nents at $T_L = 3.6$ K, for $P = 60$ W/cm 2 (top panels) and $P = 6 \times 10^2$ W/cm 2 (bottom panels).

The σ^+ component presents a monotonic dependence with magnetic field for both optical properties in Fig. 4. By increasing the magnetic field, the σ^+ exciton population diminishes, as shown in Fig. 4a, whereas the FWHM increases in Figs. 4b. This FWHM increase is expected from the short-range interaction model, according to which, $\Gamma \propto \sqrt{B}$. [36] In contrast, the σ^- component in Fig. 4 exhibits a peak response in the integrated intensity and a dip in the FWHM near $B = 1.8$ T. The peak in the σ^- exciton population disappears for $T_L \geq 20$ K, as displayed by the inset in Fig. 4a for $P = 60$ W/cm 2 . A similar effect was reported for type-II AlAs/GaAs quantum wells, [37] ascribed to the presence of coherent states, destroyed by rising temperatures. Also here, the dip in the FWHM of the σ^- component is a manifestation of increased coherence.

The applied magnetic field induces the in-plane confinement of excitons, which leads to a shrinkage of the excitonic wave function and reduces the overlap with larger in-plane disorders as represented schematically in Figs. 5a and b for $B = 0$ T and $B \neq 0$ T, respectively. The fluctuations length-scale at the interfaces can reach widths of up to 300 Å and depths up to 2.8 Å, [20] while a the excitonic Bohr radius in bulk GaAs ranges from 160 to 92 Å for magnetic fields between zero and 10 T. [38, 39] Some studies have described the modula-

tion of the linewidth as an inhomogeneous effect where interface fluctuations of two contrasting scales are averaged over the shrinking exciton radius. [33, 40] Although plausible, they cannot explain the spin modulation resolved in our experiments once the magnetic field modulation of the spin-resolved homogeneous contribution has been overlooked.

In order to consider magnetic-field-dependent decoherence mechanisms and the spin degree of freedom, the homogeneous broadening for the σ^+ and σ^- optical components can be expressed as

$$W_h^\pm(\hbar\omega_c) = \sqrt{\frac{2}{\pi} \frac{\hbar\omega_c}{\tau_p} \frac{\hbar}{\tau_p}} + \frac{\Gamma_0}{1 + \left(\frac{\hbar\omega_c}{\hbar/\tau_p}\right)^2} \eta^\pm, \quad (7)$$

where $\hbar\omega_c = \hbar eB/m^*$ is the conduction band cyclotron energy by taking into account the sharp difference between electron, m^* , and hole effective masses that allows neglecting the valence band contribution as a first approximation. The first term corresponds to the contribution of short-range scattering, [36] with τ_p being the momentum relaxation time. The second term characterizes the spin-flip scattering, [35] where Γ_0 is an intrinsic 2D-excitonic linewidth, and η^\pm takes into account the contribution from the Zeeman splitting: $\eta^+ = 1$ and $\eta^- = \exp(-g^*m^*\hbar\omega_c/k_B T_L)$, being g^* the effective Landé g -factor.

The calculated FWHM as a function of the cyclotron energy according to Eq. 7 has been displayed in Figs. 5c and d for W_h^+ and W_h^- , respectively, using $\Gamma_0 = 5$ meV and $g^*m^*/k_B T_L = 1$ meV $^{-1}$ as functions of the cyclotron energy by changing \hbar/τ_p . The energetic position of the dips is indicated with vertical dashes and labeled as $\hbar\omega_c^{\min}$. Note that the value of \hbar/τ_p , that characterizes the scattering efficiency and mobility, affects the dip position, the contrast between W_h^+ and W_h^- , and the dip depth. The latter is correlated with the lifetime and spin coherence. Figure 5e characterizes the dip position and shows that, as \hbar/τ_p increases, the W_h^\pm dip shifts to higher cyclotron energies. However, for W_h^- component, the dip appears for lower magnetic fields and this position is less sensitive to changes of \hbar/τ_p when compared to W_h^+ . The dip depth, described by $\Delta W_{h \min}^\pm = \Gamma_0 - W_{h \min}^\pm$ has been normalized with respect to Γ_0 in Fig. 5f for both W_h^+ and W_h^- . It is clear that, although $\Delta W_{h \min}^\pm$ decreases for both components as τ_p shrinks, the dip is always more prominent for W_h^- . For W_h^+ , $\Delta W_{h \min}^\pm$ drops faster and can surpass Γ_0 , turning $\Delta W_{h \min}^\pm$ negative. There is a correspondence of this contrasting theoretical picture between W_h^+ and W_h^- and the differences observed experimentally in Fig. 4b.

This model suggests that the observed behavior of the FWHM presented in Fig. 4b results mainly from the decoherence produced by short-range interactions and spin-flip scattering, respectively enhanced and suppressed by the magnetic field. At finite but low magnetic fields, the spin-flip scattering is weakened for σ^- excitonic states,

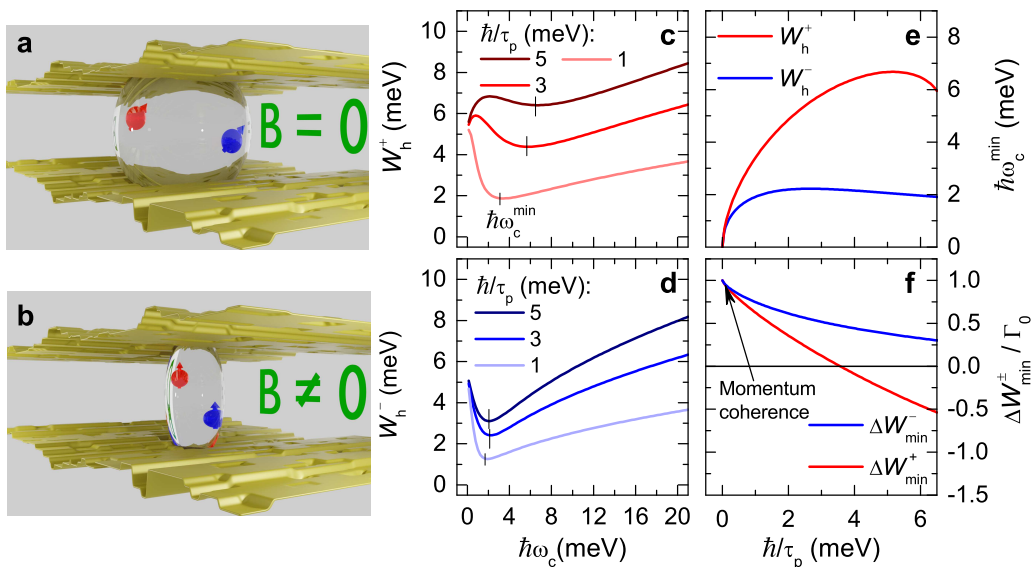


FIG. 5. Illustration of the potential fluctuations caused by the roughness along with the GaAs/AlGaAs interfaces and an electron-hole pair confined in the QW with ellipsoids symbolizing the exciton size at (a) zero ($B = 0$) and (b) non-zero ($B \neq 0$) magnetic fields. Simulated FWHM as a function of the cyclotron energy for (c) W_h^+ (red lines) and (d) W_h^- (blue lines), and for three different values of \hbar/τ_p , according to Eq. 7. (e) Dip position, $\hbar\omega_c^{\min}$, and (f) Relative depth of the dip, $\Delta W_{h \min}^{\pm}/\Gamma_0$, as a function of \hbar/τ_p . Negative values of $\Delta W_{h \min}^{\pm}/\Gamma_0$ indicate the linewidth at the dip is higher than the linewidth at a zero magnetic field, and vice versa.

at very low temperatures, due to the thermal factor, η^- , that decreases as the effective spin splitting grows. The increasing coherence translates into a reduction of the FWHM below $B = 1.8$ T. At higher magnetic fields, the short-range scattering prevails and broadens again the FWHM, producing the dip. Since our simulations show that the dip position of W_h^- is weakly affected by the momentum relaxation time, τ_p (see Fig. 5e), then it will be mainly determined by the effective Landé g -factor and the lattice temperature within the function η^- in Eq. 7. Yet, the value of τ_p affects the depth of the dip for the W_h^- component, as shown in Fig. 5f. Since the depth observed in our experiments is $\Delta W_{h \min}^-/\Gamma_0 \approx 0.038$, then a short τ_p is expected.

Our calculations predict the conditions for also obtaining a dip for W_h^+ . Its absence in our experiments indicates that the broadening induced by short-range interactions is more efficient in producing decoherence of the σ^+ excitonic states. Moreover, the simulation of the depth of the W_h^+ dip in Fig. 5f confirms that its absence is an indication of a relatively short τ_p , signature of an efficient momentum scattering and lower mobility. Consequently, to enhance the coherence of the exciton states for both W_h^+ and W_h^- components at low magnetic fields, it is necessary to reduce the efficiency of the momentum scattering, thus increasing τ_p as depicted in Fig. 5f.

IV. CONCLUSIONS

A combined experimental and theoretical study was used to investigate exciton decoherence mechanisms in GaAs/AlGaAs multiple QWs. For temperatures below 50 K and low optical densities, the hot carrier relaxation is affected by band-gap fluctuations produced by roughness at the GaAs/AlGaAs interfaces. These fluctuations favor carrier-carrier interactions that stabilize the effective temperature. To further tune the coherence, a magnetic field was applied. The PL linewidth was used to characterize the exciton coherence. Both LA-phonon interaction and band-gap fluctuations affect this parameter at cryogenic temperatures. Our results demonstrate a strong modulation of these effects with temperature and optical excitation power that allowed the deconvolution of statistical contributions to the linewidth from actual decoherence mechanisms.

At low optical power densities and lattice temperatures, the magnetic field unveiled additional scattering processes that modulate the coherence of the excitonic states. In this regime, the linewidth broadening as a function of the cyclotron energy reveals that the spin-flip scattering and short-range interactions become the main decoherence factors. The competition between these opposing contributions produces a dip in the FWHM as a function of the magnetic field, which is more pronounced for the σ^- exciton population and points out to an enhanced coherence. Its position depends on the effective Landé g -factor and the momentum relaxation time, which also determines the coherence degree. Long mo-

mentum relaxation times induce deeper FWHM dips at lower magnetic fields that are a signature of enhanced coherence.

ACKNOWLEDGMENTS

This study was financed in part by the Coordenação de Aperfeiçoamento de Pessoal de Nível Superior - Brasil

(CAPES) - Finance Code 001. The authors also acknowledge the financial support of the Fundação de Amparo à Pesquisa do Estado de São Paulo (FAPESP) - grants 2013/18719-1, 2014/19142-2, and 2018/01914-0, the Conselho Nacional de Desenvolvimento Científico e Tecnológico (CNPq), the National Science Foundation (NSF) - grant OIA-1457888. This work was also partially funded by Spanish MICINN under grant PID2019-106088RB-C3 and by the MSCA-ITN-2020 Funding Scheme from the European Union's Horizon 2020 programme under Grant agreement ID: 956548.

-
- [1] S. A. Wolf, D. D. Awschalom, R. A. Buhrman, J. M. Daughton, S. von Molnár, M. L. Roukes, A. Y. Chtchelkanova, and D. M. Treger, *Spintronics: A Spin-Based Electronics Vision for the Future*, *Science* **294**, 1488 (2001).
- [2] A. Imamoglu, D. D. Awschalom, G. Burkard, D. P. DiVincenzo, D. Loss, M. Sherwin, and A. Small, *Quantum Information Processing Using Quantum Dot Spins and Cavity QED*, *Phys. Rev. Lett.* **83**, 4204 (1999).
- [3] Y. Ohno, R. Terauchi, T. Adachi, F. Matsukura, and H. Ohno, *Spin Relaxation in GaAs(110) Quantum Wells*, *Phys. Rev. Lett.* **83**, 4196 (1999).
- [4] A. Greilich, R. Oulton, E. A. Zhukov, I. A. Yugova, D. R. Yakovlev, M. Bayer, A. Shabaev, A. L. Efros, I. A. Merkulov, V. Stavarache, D. Reuter, and A. Wieck, *Optical Control of Spin Coherence in Singly Charged (In,Ga)As/GaAs Quantum Dots*, *Phys. Rev. Lett.* **96**, 227401 (2006).
- [5] X. Xu, W. Yao, D. Xiao, and T. F. Heinz, *Spin and pseudospins in layered transition metal dichalcogenides*, *Nat. Phys.* **10**, 343 (2014).
- [6] K. Hao, G. Moody, F. Wu, C. K. Dass, L. Xu, C.-H. Chen, L. Sun, M.-Y. Li, L.-J. Li, A. H. MacDonald, *et al.*, *Direct measurement of exciton valley coherence in monolayer WSe₂*, *Nat. Phys.* **12**, 677 (2016).
- [7] M. Syperek, D. R. Yakovlev, A. Greilich, J. Misiewicz, M. Bayer, D. Reuter, and A. D. Wieck, *Spin Coherence of Holes in GaAs/(Al,Ga)As Quantum Wells*, *Phys. Rev. Lett.* **99**, 187401 (2007).
- [8] S. Ullah, G. M. Gusev, A. K. Bakarov, and F. G. G. Hernandez, *Long-lived nanosecond spin coherence in high-mobility 2DEGs confined in double and triple quantum wells*, *J. Appl. Phys.* **119**, 215701 (2016).
- [9] R. Stockill, C. Le Gall, C. Matthiesen, L. Huthmacher, E. Clarke, M. Hugues, and M. Atatüre, *Quantum dot spin coherence governed by a strained nuclear environment*, *Nat. Commun.* **7**, 1 (2016).
- [10] G. Moody, C. K. Dass, K. Hao, C.-H. Chen, L.-J. Li, A. Singh, K. Tran, G. Clark, X. Xu, G. Berghäuser, *et al.*, *Intrinsic homogeneous linewidth and broadening mechanisms of excitons in monolayer transition metal dichalcogenides*, *Nat. Commun.* **6**, 1 (2015).
- [11] G. Wang, A. Balocchi, A. V. Poshakinskiy, C. R. Zhu, S. A. Tarasenko, T. Amand, B. L. Liu, and X. Marie, *Magnetic field effect on electron spin dynamics in (110) GaAs quantum wells*, *New J. Phys.* **16**, 045008 (2014).
- [12] A. A. High, J. R. Leonard, A. T. Hammack, M. M. Fogler, L. V. Butov, A. V. Kavokin, K. L. Campman, and A. C. Gossard, *Spontaneous coherence in a cold exciton gas*, *Nature* **483**, 584 (2012).
- [13] N. S. Voronova, I. L. Kurbakov, and Y. E. Lozovik, *Bose Condensation of Long-Living Direct Excitons in an Off-Resonant Cavity*, *Phys. Rev. Lett.* **121**, 235702 (2018).
- [14] L. Butov, C. Lai, A. Ivanov, A. Gossard, and D. Chemla, *Towards Bose-Einstein condensation of excitons in potential traps*, *Nature* **417**, 47 (2002).
- [15] A. A. High, E. E. Novitskaya, L. V. Butov, M. Hanson, and A. C. Gossard, *Control of Exciton Fluxes in an Excitonic Integrated Circuit*, *Science* **321**, 229 (2008), <https://science.sciencemag.org/content/321/5886/229.full.pdf>.
- [16] L. W. Molenkamp, G. E. W. Bauer, R. Eppenga, and C. T. Foxon, *Exciton binding energy in (Al,Ga)As quantum wells: Effects of crystal orientation and envelope-function symmetry*, *Phys. Rev. B* **38**, 6147 (1988).
- [17] Y. Kajikawa, *Comparison of 1s-2s exciton-energy splittings between (001) and (111) GaAs/Al_xGa_{1-x}As quantum wells*, *Phys. Rev. B* **48**, 7935 (1993).
- [18] J. Shah and R. C. C. Leite, *Radiative Recombination from Photoexcited Hot Carriers in GaAs*, *Phys. Rev. Lett.* **22**, 1304 (1969).
- [19] R. Hellmann, M. Koch, J. Feldmann, S. Cundiff, E. Göbel, D. Yakovlev, A. Waag, and G. Landwehr, *Dephasing of excitons in a CdTe/Cd_{0.86}Mn_{0.14}Te multiple quantum well*, *J. Cryst. Growth* **138**, 791 (1994).
- [20] J. Behrend, M. Wassermeier, W. Braun, P. Krispin, and K. H. Ploog, *Formation of GaAs/AlAs(001) interfaces studied by scanning tunneling microscopy*, *Phys. Rev. B* **53**, 9907 (1996).
- [21] V. Srinivas, J. Hryniewicz, Y. J. Chen, and C. E. C. Wood, *Intrinsic linewidths and radiative lifetimes of free excitons in GaAs quantum wells*, *Phys. Rev. B* **46**, 10193 (1992).
- [22] R. Pässler, *Basic Model Relations for Temperature Dependencies of Fundamental Energy Gaps in Semiconductors*, *Phys. Status Solidi B* **200**, 155 (1997).
- [23] O. Madelung, *Semiconductors: Data handbook (CD-ROM)*, 3rd ed. (Springer, 2004).
- [24] M. D. Teodoro, I. F. L. Dias, E. Laureto, J. L. Duarte, P. P. González-Borrero, S. A. Lourenço, I. Mazzaro, E. Marega, and G. J. Salamo, *Substrate orientation effect on potential fluctuations in multiquantum wells of GaAs/AlGaAs*, *J. Appl. Phys.* **103**, 093508 (2008).
- [25] J. Mattheis, U. Rau, and J. H. Werner, *Light absorption and emission in semiconductors with band*

- gap fluctuations—A study on Cu(In,Ga)Se₂ thin films, *J. Appl. Phys.* **101**, 113519 (2007).
- [26] J. Christen and D. Bimberg, Line shapes of intersubband and excitonic recombination in quantum wells: Influence of final-state interaction, statistical broadening, and momentum conservation, *Phys. Rev. B* **42**, 7213 (1990).
- [27] L. Andrews and S. of Photo-optical Instrumentation Engineers, *Special Functions of Mathematics for Engineers*, 2nd ed., Online access with subscription: SPIE Digital Library (SPIE Optical Engineering Press, Washington, 1998).
- [28] E. Whiting, An empirical approximation to the Voigt profile, *J. Quant. Spectrosc. Radiat. Transfer* **8**, 1379 (1968).
- [29] J. Olivero and R. Longbothum, Empirical fits to the Voigt line width: A brief review, *J. Quant. Spectrosc. Radiat. Transfer* **17**, 233 (1977).
- [30] J. Lee, E. S. Koteles, and M. O. Vassell, Luminescence linewidths of excitons in GaAs quantum wells below 150 K, *Phys. Rev. B* **33**, 5512 (1986).
- [31] H. P. Wagner, A. Schätz, R. Maier, W. Langbein, and J. M. Hvam, Coherent optical nonlinearities and phase relaxation of quasi-three-dimensional and quasi-two-dimensional excitons in ZnS_xSe_{1-x}/ZnSe structures, *Phys. Rev. B* **56**, 12581 (1997).
- [32] I. Aksenov, J. Kusano, Y. Aoyagi, T. Sugano, T. Yasuda, and Y. Segawa, Effect of a magnetic field on the excitonic luminescence line shape in a quantum well, *Phys. Rev. B* **51**, 4278 (1995).
- [33] B. Bansal, M. Hayne, B. M. Arora, and V. V. Moshchalkov, Magnetic field-dependent photoluminescence linewidths as a probe of disorder length scales in quantum wells, *Appl. Phys. Lett.* **91**, 251108 (2007).
- [34] X. Chen, Z. Xu, Y. Zhou, L. Zhu, J. Chen, and J. Shao, Evaluating interface roughness and micro-fluctuation potential of InAs/GaSb superlattices by mid-infrared magnetophotoluminescence, *Appl. Phys. Lett.* **117**, 081104 (2020).
- [35] M. M. Glazov, Magnetic field effects on spin relaxation in heterostructures, *Phys. Rev. B* **70**, 195314 (2004).
- [36] T. Ando and Y. Uemura, Theory of Quantum Transport in a Two-Dimensional Electron System under Magnetic Fields. I. Characteristics of Level Broadening and Transport under Strong Fields, *J. Phys. Soc. Jpn.* **36**, 959 (1974).
- [37] L. V. Butov, A. Zrenner, G. Abstreiter, G. Böhm, and G. Weimann, Condensation of Indirect Excitons in Coupled AlAs/GaAs Quantum Wells, *Phys. Rev. Lett.* **73**, 304 (1994).
- [38] P. Harrison *et al.*, *Quantum wells, wires and dots*, 4th ed. (Wiley Online Library, 2001).
- [39] P. Stepnicki, B. Piętko, F. m. c. Morier-Genoud, B. Deveaud, and M. Matuszewski, Analytical method for determining quantum well exciton properties in a magnetic field, *Phys. Rev. B* **91**, 195302 (2015).
- [40] S. Harrison, M. P. Young, P. D. Hodgson, R. J. Young, M. Hayne, L. Danos, A. Schliwa, A. Strittmatter, A. Lenz, H. Eisele, U. W. Pohl, and D. Bimberg, Heterodimensional charge-carrier confinement in stacked submonolayer inas in gaas, *Phys. Rev. B* **93**, 085302 (2016).